Meteoritics & Planetary Science 41, Nr 10, 1483–1495 (2006)
Abstract available online at http://meteoritics.org

The planforms of low-angle impact craters in the northern hemisphere of Mars

Robert R. HERRICK* and Katie K. HESSEN

Geophysical Institute, University of Alaska–Fairbanks, Fairbanks, Alaska, USA
*Corresponding author. E-mail: rherrick@gi.alaska.edu

(Received 17 October 2005; revision accepted 26 July 2006)

Abstract–We have surveyed Martian impact craters greater than 5 km in diameter using Viking and thermal emission imaging system (THEMIS) imagery to evaluate how the planform of the rim and ejecta changes with decreasing impact angle. We infer the impact angles at which the changes occur by assuming a $\sin^2\Theta$ dependence for the cumulative fraction of craters forming below angle Θ. At impact angles less than ~40° from horizontal, the ejecta become offset downrange relative to the crater rim. As the impact angle decreases to less than ~20°, the ejecta begin to concentrate in the cross-range direction and a "forbidden zone" that is void of ejecta develops in the uprange direction. At angles less than ~10°, a "butterfly" ejecta pattern is generated by the presence of downrange and uprange forbidden zones, and the rim planform becomes elliptical with the major axis oriented along the projectile's direction of travel. The uprange forbidden zone appears as a "V" curving outward from the rim, but the downrange forbidden zone is a straight-edged wedge. Although fresh Martian craters greater than 5 km in diameter have ramparts indicative of surface ejecta flow, the ejecta planforms and the angles at which they occur are very similar to those for lunar craters and laboratory impacts conducted in a dry vacuum. The planforms are different from those for Venusian craters and experimental impacts in a dense atmosphere. We interpret our results to indicate that Martian ejecta are first emplaced predominantly ballistically and then experience modest surface flow.

INTRODUCTION

All planetary impacts occur at nonvertical angles, and for near-horizontal or "oblique" impacts, the resulting shape and appearance of the crater and its ejecta can be very asymmetric (Gault and Wedekind 1978; Pierazzo and Melosh 2000). Understanding how the cratering process changes for increasingly oblique impacts is critical to understanding planetary impact crater formation and to utilizing the cratering record to study the geologic history of a planet. As illustrated in laboratory experiments (e.g., Gault and Wedekind 1978; Schultz 1992b) and through comparison of lunar and Venusian craters (Schultz 1992b; Herrick and Forsberg-Taylor 2003), the nature of asymmetries associated with oblique impacts and their angle of occurrence can vary dramatically with target properties. For example, the Moon-Venus comparison (Herrick and Forsberg-Taylor 2003) highlighted the differences between impacts in a vacuum and those occurring on a planet with a dense atmosphere. Detailed examination of oblique impact forms on Mars has the potential to provide unique constraints on the general cratering process and the particular mechanism of Martian rampart crater formation.

Gault and Wedekind (1978) conducted a series of experimental hypervelocity impacts in a vacuum that identified general changes in crater properties with decreasing impact angle. As impact angle decreased, a region void of ejecta (a "forbidden zone") developed first uprange and then downrange, culminating in a "butterfly" pattern for impacts <5° from horizontal. Accompanying these changes in ejecta pattern were depressions in the crater rim, first in the uprange and then in the downrange direction. Craters with a butterfly ejecta pattern were also elliptical with the long axis in the impact direction. Gault and Wedekind (1978) showed examples of craters from the Moon and Mars that have an appearance similar to the experimental craters.

Schultz (1992b) conducted oblique impact experiments in an atmosphere and compared them to Venusian craters. In the presence of a dense atmosphere, the ejecta are entrained and emplaced as ground-hugging flows. Asymmetries in the ejecta planform occurred at much higher impact angles in an atmosphere than they did in a vacuum. Before impact the incoming projectile imparts momentum into the atmosphere, and as a consequence ejecta are swept downrange during the excavation process. While an uprange forbidden zone develops that is similar to the vacuum case, downrange

forbidden zones do not occur for any impact angle. Schultz (1992b) used the experimental work to identify a sequence in Venusian crater appearance for increasingly oblique impacts and to estimate the transition angles between those crater forms.

Although planetary examples were found that qualitatively match the appearance of the experimental impacts, it is not necessarily true that the planetary craters were formed with the same impact angle as the most similar experimental crater. Because impactors are expected to enter a planet's atmosphere from random directions at angles with a predictable frequency distribution (Shoemaker 1962), impact angles can be inferred from the percentages of the total crater population that have the various oblique shapes and ejecta planforms. Schultz and Lutz-Garihan (1982) estimated the percentage of the Martian crater population that were "grazing impacts," meaning those craters whose appearance resembled laboratory impacts at <5°. They found a higher percentage of grazing impacts than anticipated and hypothesized that there was an excess of lowest-angle impacts caused by a population of moonlets spiraling into the planet. Bottke et al. (2000) used an elliptical crater rim as an indicator of a grazing impact, and they determined the percentage of elliptical craters on Mars, Venus, and the Moon. Their results for Mars were consistent with the findings of Schultz and Lutz-Garihan (1982), but they found similar percentages of elliptical craters on Venus and the Moon. Rather than interpreting their results as indicating an excess of low-angle impacts on all three planets, Bottke et al. (2000) concluded that planetary craters become elliptical at higher impact angles (~12°) than in the Gault and Wedekind (1978) experiments.

Herrick and Forsberg-Taylor (2003) surveyed crater shapes and ejecta planforms on Venus and the Moon and inferred the progression with decreasing impact angle on those two bodies. The progression in ejecta planform and crater shape and the angles at which various transitions occur on Venus and the Moon are broadly consistent with those observed in experimental work in a vacuum (Gault and Wedekind 1978) and in an atmosphere (Schultz 1992b), respectively. Asymmetries in the ejecta planform occur at much higher impact angles on Venus than on the Moon. As impact angle decreases on both planets, first the uprange and then the downrange rim go to zero elevation, while the cross-range rim elevation remains unchanged. The Herrick and Forsberg-Taylor (2003) surveys are consistent with the Bottke et al. (2000) results for grazing impacts, but the number of craters surveyed are far fewer because Herrick and Forsberg-Taylor (2003) considered only well-preserved craters. At small crater diameters on Venus (<15 km), meteoroid breakup and dispersal becomes a significant fraction of crater diameter (Herrick and Phillips 1994), and a variety of crater shapes and planforms can be observed that are consistent with clustered, oblique impact experiments (Schultz and Gault 1985).

Most well-preserved larger impact craters on Mars (diameter D > 5 km) show clear evidence of flow during ejecta emplacement that results in features known as "rampart craters." The variety of mechanisms suggested for how these distinctive ejecta blankets form invoke different roles for the atmosphere and subsurface volatiles. The possibilities for the role of the atmosphere range from significant, near-rim entrainment in vortices to post-ballistic processes such as gas entrainment in flows and recovery winds scouring the post-emplacement surface (Schultz and Gault 1979; Schultz 1992a; Barnouin-Jha and Schultz 1996, 1998). Involvement of subsurface volatiles could range from producing mud flows that originate near the rim to providing lubrication for flows that essentially begin after lunar-like ballistic deposition (e.g., Carr et al. 1977; Gault and Greeley 1978; Barnouin-Jha et al. 2005). While these mechanisms will all produce radially symmetric ejecta blankets for near-vertical impacts, clearly the nature of the asymmetries with oblique impact will vary between mechanisms. In this work, we survey the Martian impact crater population and characterize how crater appearance changes with decreasing impact angle. In general terms, we expect that mechanisms that have flow beginning after mostly ballistic deposition would generate planforms and transition angles for oblique impacts that most resemble vacuum conditions.

METHODOLOGY

In this work, we use a methodology similar to that used in Herrick and Forsberg-Taylor (2003). We surveyed a large number of craters within a given area in a manner that allowed us to attribute the variations in crater appearance to impact angle. In this case, we chose to survey craters >5 km in diameter because it allowed us to use the *Catalog of Large Martian Craters*, compiled by Nadine Barlow and colleagues (e.g., Barlow et al. 2000; Barlow 2000; Barlow and Bradley 1990), as a starting point. Craters this large can be characterized with the mosaicked Viking data, and all of these craters are rampart craters. To minimize terrain effects on ejecta emplacement, we restricted ourselves to craters in the northern lowlands (survey area 30–90°N, all longitudes, and 0–30°N, 50–280°W) and do not include craters obviously located on significant topographic slopes or rugged terrain. The surveys in Herrick and Forsberg-Taylor (2003) had small populations because Venus does not have many craters, and on the Moon it is difficult for most craters to distinguish the ejecta blanket from the underlying terrain. On Mars the situation is improved because the northern lowlands provide an unsaturated flat surface with abundant craters, and the ramparts make the ejecta planforms distinguishable from the underlying terrain.

As we identified impact craters in the survey area that have preserved ejecta blankets, we began an iterative process of placing the craters within categories indicative of decreasing impact angle. The categories are derived from the

Table 1. Classification of Martian impact craters with $D > 5$ km for entire survey population. "90% CI" is the 90% confidence interval for the cumulative fraction (e.g., Johnson 1973); that range is used to calculate the range in transition angles from Equation 1.

Description	Number of craters	Cumulative fraction	90% CI	Transition angle
Butterfly	9	0.030	0.016	7–12°
Forbidden zone	11	0.066	0.023	12–17°
Offset and concentrated cross-range	9	0.097	0.028	15–21°
Offset	66	0.317	0.044	31–37°
Symmetric	205	1.000		
Total	300			

craters by interpreting a logical sequence through comparison with experimental studies. The categories were refined as the survey continued and craters were reclassified. After the identification and categorization process concluded, we can infer impact angle using the formula for the percentage P of meteoroids entering the atmosphere below an angle Θ for a random population (Shoemaker 1962):

$$P = \sin^2\Theta \quad (1)$$

Using Equation 1 to estimate impact angle assumes that there is no dependence of crater diameter on impact angle. The expectation that cratering efficiency decreases as the impact angle becomes more horizontal would have the general effect of increasing the exponent in Equation 1 and thus lowering the percentage of craters attributable to near-horizontal impacts. Modifications to Equation 1 for an angular dependence of cratering efficiency are examined in Herrick and Forsberg-Taylor (2003). As discussed above, Equation 1 would be invalid if there is a significant population of moonlets spiraling in and impacting at low angles. Other possible complications from atmospheric filtering of meteoroids or a population of secondary craters are expected only to be important on Mars for crater diameters much smaller than we are considering.

Viking imagery was used for the initial classification because of its uniformity of image resolution and its universal coverage. More recently, however, a number of imagery data sets have been collected for Mars that provide varying degrees of areal coverage at higher resolutions than the Viking data. In particular, the Thermal Emission Imaging System (THEMIS) instrument on the Mars Odyssey spacecraft has imaged a substantial portion of the planet at ~20 m resolution in several visual bands and ~100 m resolution in the infrared. The infrared images taken during the Martian daytime are very similar in appearance to panchromatic visual images, and their coverage is nearly universal in the study area. Most of the craters in this study had only partial coverage in the higher-resolution THEMIS visual imagery. A mosaicked form of THEMIS data has not been publicly released yet, but the data are available as individual map-projected image strips that can be tiled together to create a mosaic. For the subset of craters that had nonsymmetric ejecta blankets, we looked in detail at available THEMIS daytime IR and visual images, and we summarize our observations below.

RESULTS

Planform Categories

Table 1 summarizes the results of our survey and Fig. 1 shows type examples that illustrate our interpreted progression with decreasing impact angle. We infer the following forms with increasingly horizontal impact angle.

Symmetric

The crater rim is circular and the ejecta planform is axisymmetric.

Offset

Both the crater rim and the ejecta are generally circular in planform, but their center points are offset. The direction that the ejecta are offset relative to the crater center is inferred to be the downrange direction. For craters with multiple ejecta lobes, the inner lobe generally seems to extend radially from the rim a constant fraction of the distance of the outer lobe. However, in a few cases for this category and the other asymmetric crater forms, the inner lobe appears to extend as far or farther than the outer lobe in the uprange direction.

A variety of interior morphologies (central peak, central pits, summit pits, etc.) are observed for these craters, and there are no obvious trends of interior asymmetries (central peak offset, preferential downrange terracing, etc.).

Offset and Concentrated in the Cross-Range Direction

The crater rim is circular but the ejecta are grossly elliptical in planform. The major axis of the ejecta ellipse is inferred to be the cross-range direction. The direction that the ejecta are offset relative to the crater center is inferred to be the downrange direction. There were three craters in this category with well-preserved central structures, and we interpret all of them to have a central floor pit. Unfortunately, there are too few craters to evaluate whether or not the presence of a central pit is a universal trait for large craters in this category.

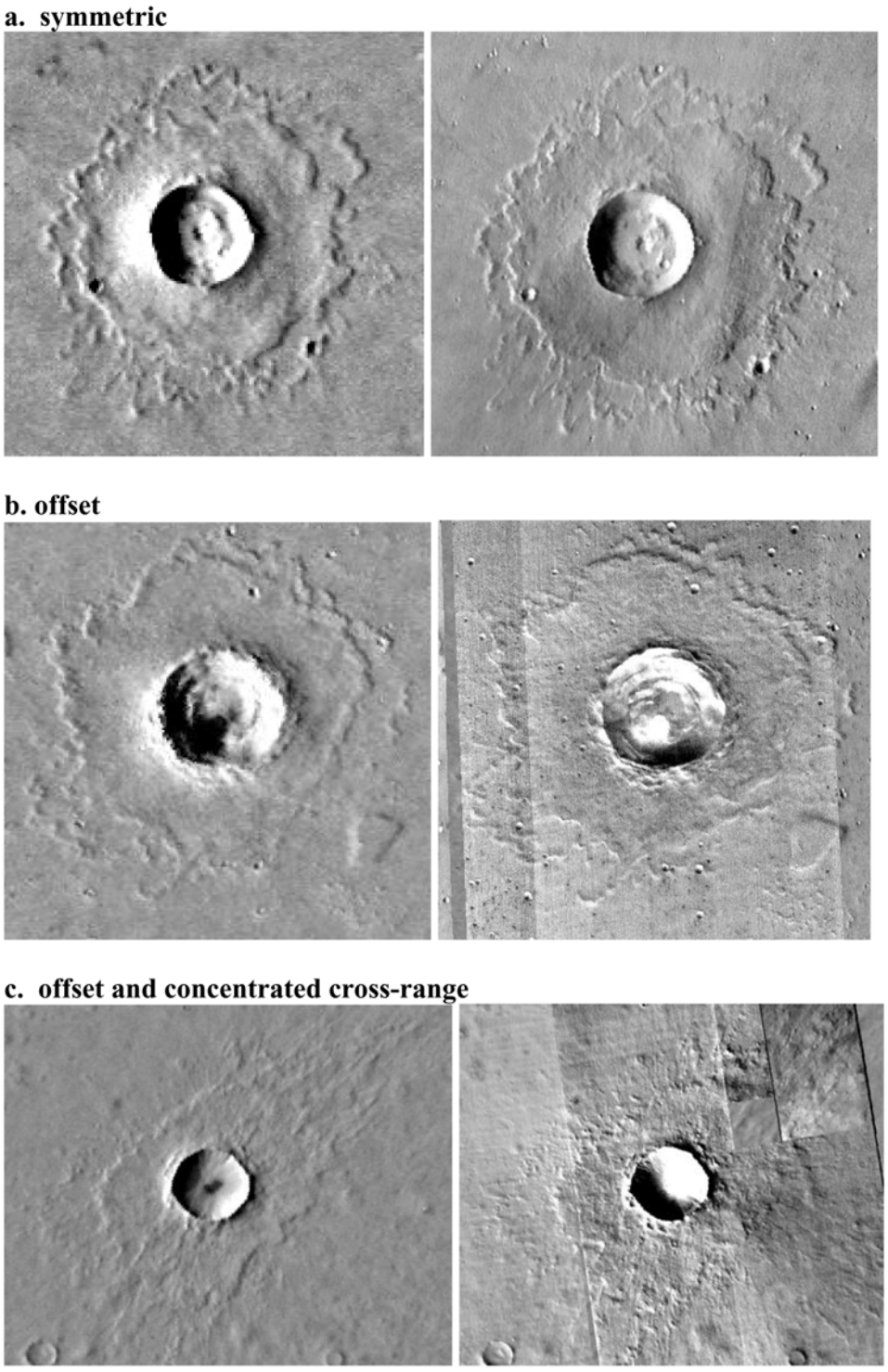

Fig. 1. Selected examples illustrating the progression of Martian landforms as impact angle becomes increasingly horizontal for craters with $D > 5$ km. The left image of each pair is from the Viking Mars Digital Image Mosaic, Version 2 (MDIM2), and the right image shows the crater in THEMIS imagery. Diameters are as listed in the *Catalog of Large Martian Craters* (Barlow 2000). The progression of butterfly craters from (f) to (i) shows ricocheted material increasingly contained within the final crater. The butterfly crater in (f) has a small uprange companion crater interpreted to result from impact of a fragment from the primary meteoroid. Azimuth (A) of interpreted impact direction in degrees clockwise from north. a) Symmetric: 35.4°N, 311.2°E, $D = 10$ km. b) Offset: 25.5°N, 103.1°E, $D = 13$ km, $A = 315°$. c) Offset and concentrated cross-range: 63.8°N, 292.0°E, $D = 17$ km, $A = 319°$.

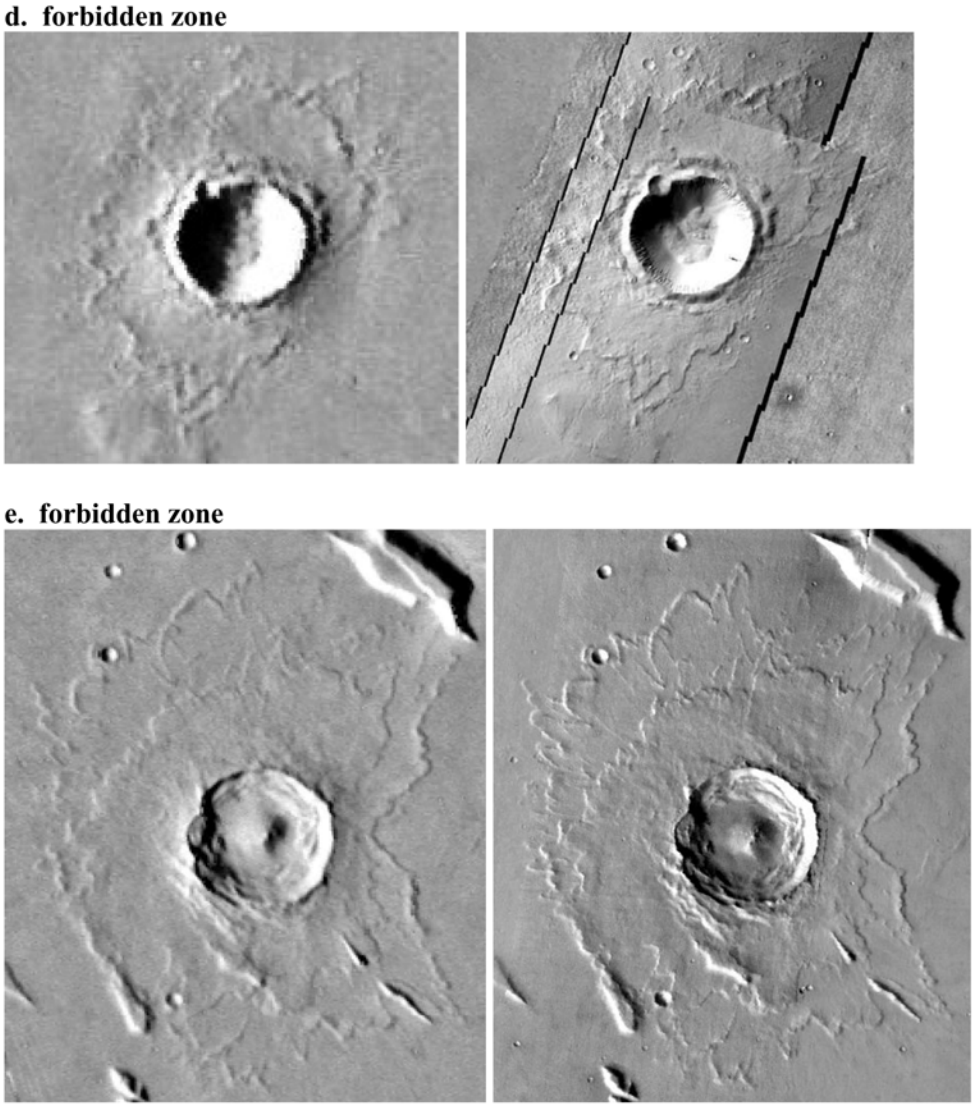

Fig. 1. *Continued.* Azimuth (*A*) of interpreted impact direction in degrees clockwise from north. d) Forbidden zone: 24.2°N, 116.8°E, *D* = 10 km, *A* = 310°. e) Forbidden zone: 18.1°N, 160.9°E, *D* = 15 km, *A* = 271°.

Uprange Forbidden Zone

The ejecta are concentrated in what is inferred to be the downrange and cross-range directions. In the uprange direction a zone of avoidance, or "forbidden zone" develops with the shape of an outward-curving "V" with its apex at the crater rim. The crater rim is circular and appears axisymmetric. These craters shown no trends for interior asymmetries. There are five craters in this category with well-preserved central structures; four have a single central peak and one has a central floor pit.

Butterfly Pattern

Forbidden zones are developed in both the uprange and downrange directions, and ejecta are concentrated in two cross-range lobes (like the wings of a butterfly). One forbidden zone forms a straight-edged angle, and the other has the outward curving "V" shape; we interpret the latter as being indicative of the uprange direction. In some cases the apex of the uprange and downrange forbidden zones is at the rim, but in other cases the apex is slightly outward. The crater rims for all of the Martian butterfly craters are elliptical with the major axis aligned along the inferred projectile direction of travel. Ellipticities (ratio of major to minor axis) for the butterfly craters range from 1.1 to 1.8, with a mean of 1.4 and standard deviation of 0.3. The crater rims are circular for all other higher-angle forms.

Although small numbers of butterfly craters are observed, there appears to be a progression regarding what we interpret to be ricocheted material. Also sometimes referred to as impactor decapitation, some of the impacting material effectively skips off the surface after the first impact and then impacts a second time downrange. The progression is from

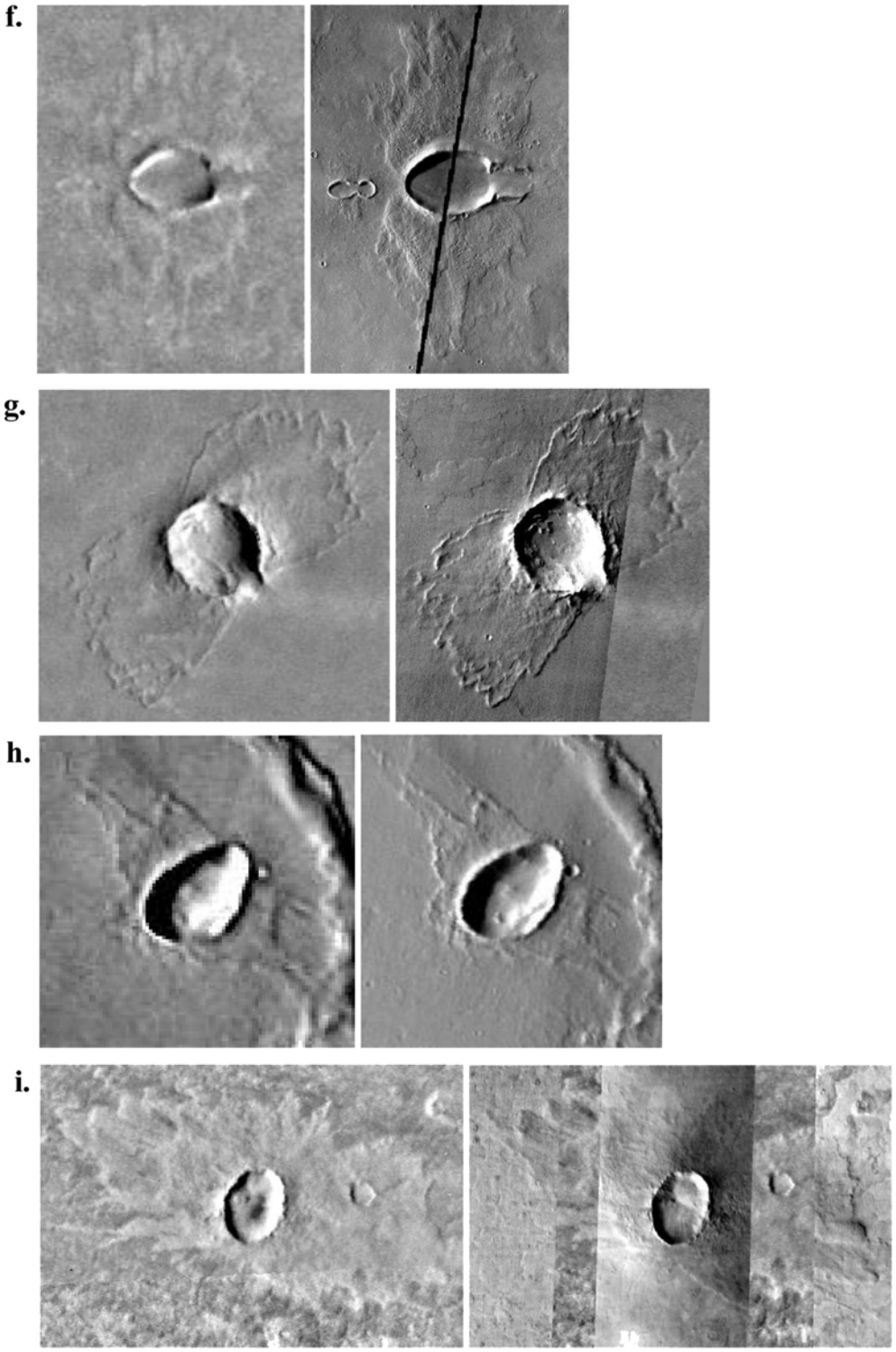

Fig. 1. *Continued.* Selected examples illustrating the progression of Martian landforms as impact angle becomes increasingly horizontal for craters with $D > 5$ km. The left image of each pair is from the Viking Mars Digital Image Mosaic, Version 2 (MDIM2), and the right image shows the crater in THEMIS imagery. Diameters are as listed in the *Catalog of Large Martian Craters* (Barlow 2000). The progression of butterfly craters from (f) to (i) shows ricocheted material increasingly contained within the final crater. The butterfly crater in (f) has a small uprange companion crater interpreted to result from impact of a fragment from the primary meteoroid. Azimuth (A) of interpreted impact direction in degrees clockwise from north. f) Butterfly: 40.5°N, 222.5°E, D = 12 km, A = 89°. g) Butterfly: 9.2°N, 279.6°E, D = 13 km, A = 139°. h) Butterfly: 21.6°N, 280.8°E, D = 7.0 km, A = 51°. i) Butterfly: 48.0°N, 323.8°E, D = 17 km, A = 19°.

the ricochet creating a nearly separate crater downrange, to interrupting development of a downrange rim, to being entirely contained within the crater (Figs. 1f–i). There are no apparent ejecta flows emanating from the extension of the crater structure associated with the ricochet. Associated with the progression in rim planform is a transition from an avoidance zone that extends straight from the rim to the presence of a small lobe of downrange ejecta. This transition may reflect the influence of the ricochet material on the ejecta emplacement process. Butterfly craters always have an uprange rim, but in some cases they lack a downrange rim in the area we interpret to be affected by ricochet.

There are also interesting changes with increasing crater diameter that are observable in the butterfly craters. The ejecta lobes of the two smallest butterfly craters (D = 7.0 and 10.5 km) have very irregular boundaries (e.g., Fig. 1h). This may be because we are seeing only the inner lobes of an eroded double-layered crater, and these should be more irregular than the outer lobes (see discussion below regarding ejecta blankets with short extent). The three largest butterfly craters (D = 28.1, 30.6, and 33.4 km) have an interior structure that includes a linear ridge that is subparallel to the major axis of the crater rim. In one case this interior ridge truncates at the crater wall, and yet there is no expression of the ridge exterior to the crater (Fig. 2). This suggests that there is a sharp lateral transition from the interior collapsed/rebounded material in a complex crater to the undisplaced surrounding strata.

Finally, two of the butterfly craters appear to have small uprange companion craters (e.g., Fig. 1f) that we interpret as resulting from the impact of a fragment of the primary meteoroid. Meteoroid fragmentation in an atmosphere and production of a crater field has been inferred on Earth and Venus (Passey and Melosh 1980; Herrick and Phillips 1994). Schultz and Lutz-Garihan (1982) suggested that the craters in Fig. 1f resulted from tidal disruption of a single impactor. While we cannot rule out tidal disruption as a cause of meteoroid fragmentation, we suggest that the separation of the craters in Fig. 1f is primarily due to the differential effects of atmospheric drag on two meteoroid fragments. Small fragments do not travel as far downrange in the atmosphere because they are slowed more by atmospheric drag (Passey and Melosh 1980), and consequently the largest crater in a field is also the furthest downrange. Unlike on Earth and Venus, there was no cross-range spread of the fragments for the Martian craters.

Discussion

We saw no differences between crater types in the transition diameters for interior complexity (e.g., onset of central peaks, terracing). Other than the aforementioned radial ridges, there were no consistent deviations from an axially symmetric crater interior for the different crater forms.

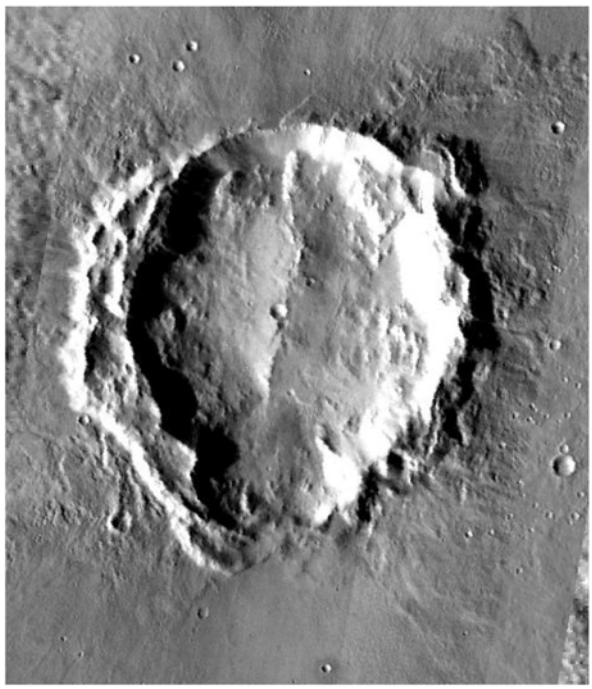

Fig. 2. The interior of a butterfly crater at 29.7°N, 87.3°E (D = 30.6 km, A = 181°). The ridge that runs subparallel to the impact direction truncates against the crater wall but has no surface expression exterior to the crater.

We also saw no occurrence of different crater forms being preferentially single-layered, double-layered, or multiple-layered, according to the classification scheme of Barlow et al. (2000). We reclassified many of the craters in Barlow and Bradley (1990) from single-layered to double-layered after examination utilizing THEMIS imagery; in several cases erosional remnants from a second layer were evident in the THEMIS imagery but not in the Viking imagery (Barlow 2005 also noted reclassifying many craters with the THEMIS imagery).

We consider the position in the sequence of the “offset and concentrated in the cross-range direction” category to be somewhat ambiguous, as there are a few craters with forbidden zones for which the ejecta extend in the downrange direction as much as in the cross-range direction (e.g., Fig. 1e). We favor the stated sequence because our assessment of the overall Martian population and the experiments of Gault and Wedekind (1978) is that ejecta start concentrating in the cross-range direction for slightly more vertical impact angles than those for which an uprange forbidden zone clearly starts developing.

While we have confidence that we have correctly identified the general sequence in crater planform with decreasing impact angle, there are some important caveats that must be discussed with respect to the numbers of craters in Table 1. One of the problems becomes clear if the locations of the craters in our survey are plotted according to their

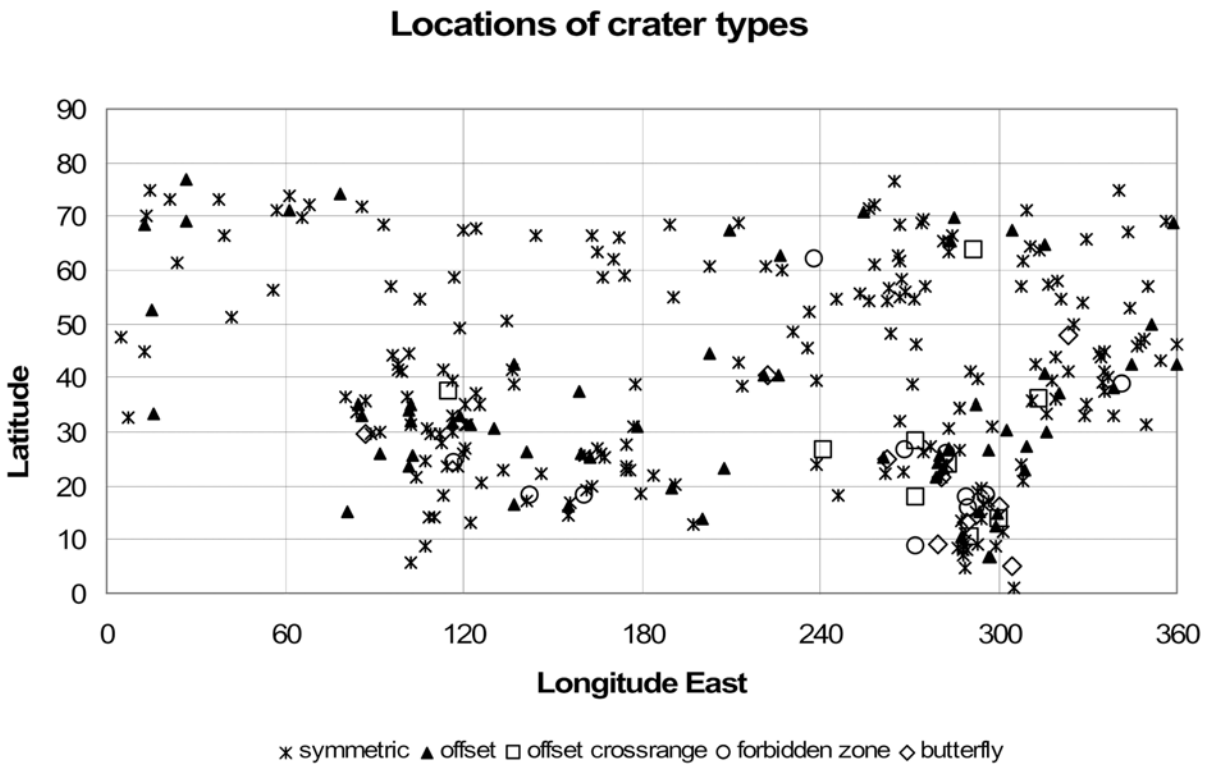

Fig. 3. The geographic locations of craters in the survey.

geographic coordinates (Fig. 3). All but two of the lowest-angle impact forms occur below 50°N latitude. The absence of highly asymmetric craters at high latitudes could reflect a genuine change in the nature of the impactor population with latitude. Moonlets spiraling into the planet are most likely to have near-equatorial orbits, so a scenario where significant numbers of craters are produced by moonlets could generate a latitudinal dependence for low-angle impacts (Schultz and Lutz-Garihan 1982).

Instead, we favor an explanation for the absence of high-latitude oblique impact forms that is based on the unusual terrain characteristics of the Vastitas Borealis region on Mars that is above 50°N latitude. A significant portion of the impact craters in Vastitas Borealis look like that shown in Fig. 4d. For inclusion in our survey we required that the boundary of the ejecta blanket of a crater be well-defined. While there is a clearly defined boundary to the ejecta for many of the northern craters, it is not clear that this represents the original full extent of the ejecta or even a structure that originally would have been visible. The sequence in Fig. 4 suggests that craters with a current single-layered blanket with no ramparts may be the erosional remnant of a more extensive ejecta blanket, but this is not necessarily always the case (the article in this issue by Barlow discusses this topic as well). Like some terrestrial impact structures, such topographically elevated blankets could be an erosional remnant of some interior feature that originally had no topographic expression. Alternatively, in some cases there may be something unusual about the initial depositional environment (submarine, glacier-covered) that prohibited the highly asymmetric forms seen at lower latitudes.

Figure 5 shows the diameter dependence of the crater forms for the full survey and the subpopulations above and below 50°N. For the craters below 50°N, the ratios of highly oblique to symmetric crater forms are diameter-independent within error bounds, but the data above 50°N are most easily interpreted as an overabundance of symmetric craters in the 8–16 km diameter range. This observation is unlikely to result from significant numbers of moonlets within the impactor population. The larger crater diameter ranges should be most affected by a moonlet population because a moonlet must be large enough to generate a tidal bulge on Mars in order to spiral into the planet. Thus, if there was a significant population of moonlets and they impacted more frequently at lower latitudes, then we would expect an overabundance of high-latitude symmetric craters to be most pronounced for large-diameter craters rather than craters in the 8–16 km diameter range.

As an additional test, we can look at the directionality of the lowest angle impacts. We expect that impacts resulting from moonlets spiraling into the planet would be at low angle and equatorial. However, there is no preferential impact direction for the butterfly craters or the forbidden zone craters (Fig. 6).

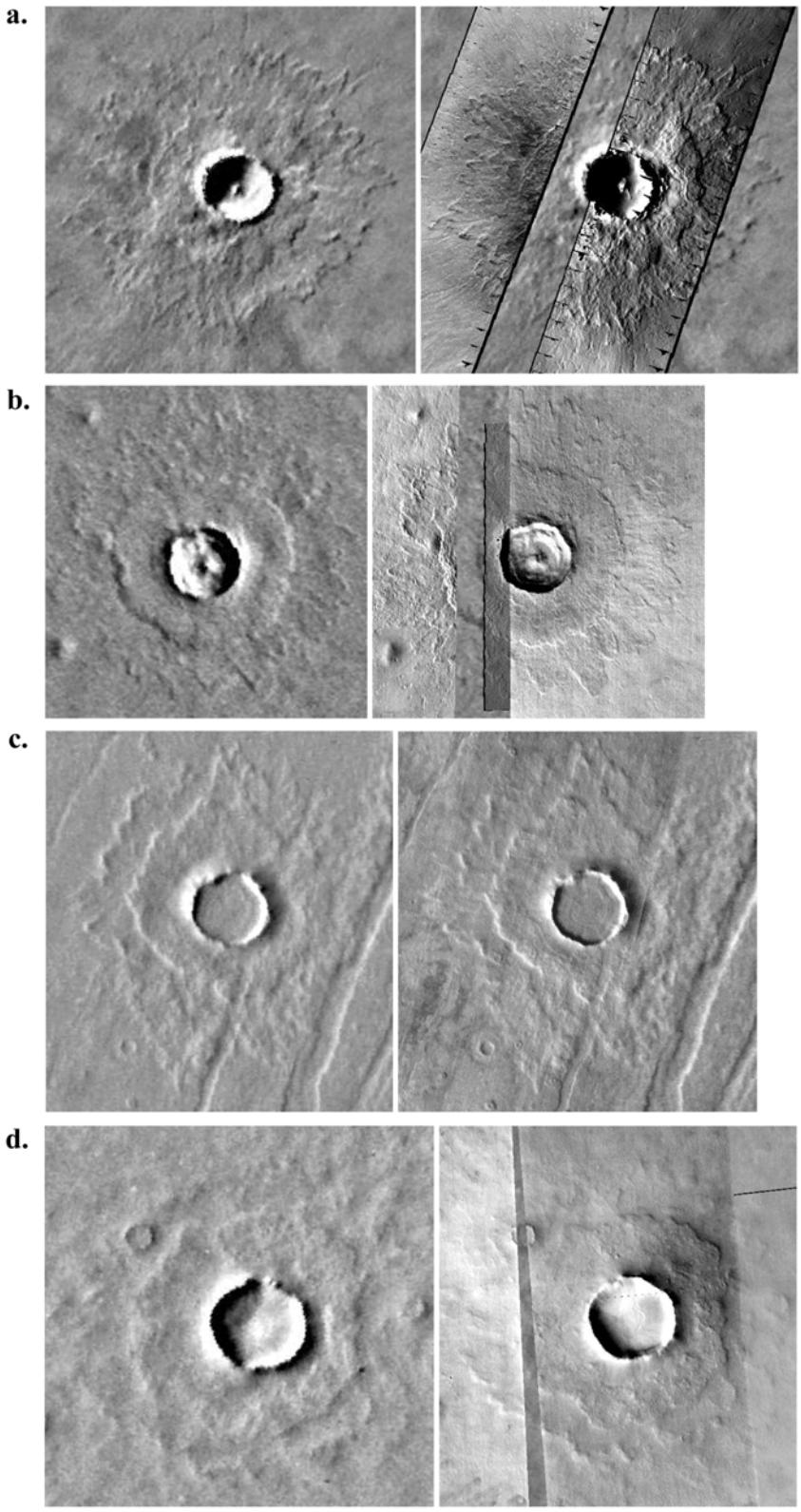

Fig. 4. Craters 10–12 km in diameter with symmetric ejecta blankets located above 50°N that illustrate a potential degradational sequence in Vastitas Borealis. As in Fig. 1, the left images are from MDIM2 and the right images are from THEMIS. a) 73.0°N, 38.4°E; b) 54.5°N, 190.6°E; c) 56.4°N, 263.1°E; and d) 68.6°N, 12.9°E.

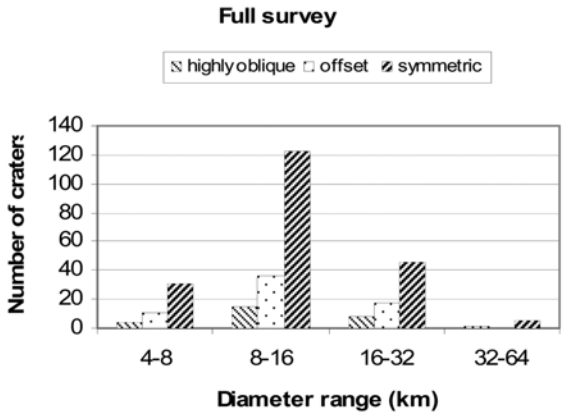

a.

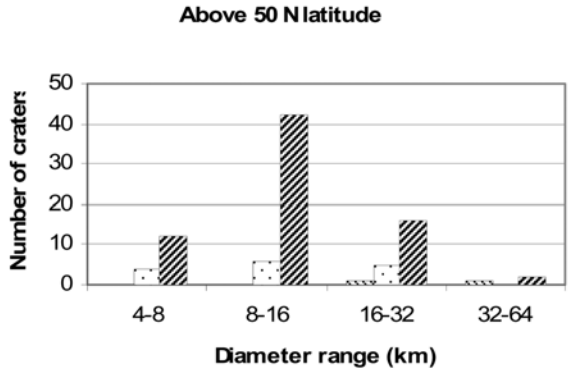

b.

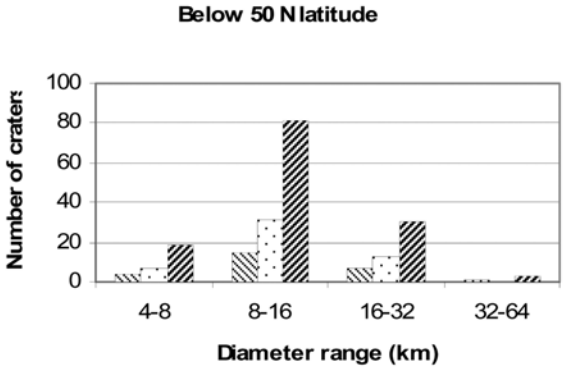

c.

Fig. 5. The size dependence of crater categories for a) full survey, b) craters above 50°N, and c) craters below 50°N. The "highly oblique" column sums the "butterfly," "forbidden zone," and "offset and concentrated cross-range" categories of Tables 1 and 2. One standard deviation error, assuming Poisson statistics, is the square root of the total in each category.

We hypothesize that erosional processes at high latitudes are such that it is harder to identify and classify degraded asymmetric crater forms than symmetric forms, and that this difference is more pronounced at smaller diameters. Further, the erosional remnants of a highly asymmetric crater may appear more nearly symmetric than the original ejecta blanket. For example, if erosion had caused only the inner ejecta lobe for the crater in Fig. 7 to be preserved, then we might have classified this crater as "offset" rather than "uprange forbidden zone." While degradational processes are certainly affecting our survey population below 50°N, the more random spatial pattern and the lack of size dependence for the different crater forms gives us confidence that our results for this subpopulation are adequately robust. The unusual properties of impact craters in the Vastitas Borealis region have been noted in a variety of different contexts (e.g., Schultz and Lutz-Garihan 1982; Barlow and Bradley 1990; Tanaka et al. 2003), so we think it is reasonable to exclude the higher latitude data when drawing general conclusions.

As a final caveat, while conducting our survey we noted that about 10% of the craters in the population below 50°N had an ejecta extent that seemed unusually short (Fig. 8). In some cases, it seems possible that the short extent is caused by the blanket being the erosional remnant of a larger blanket, but in other cases, the short extent of the ejecta appears to be a primary feature. We do not have a ready explanation for the cause of these short ejecta blankets, so we cannot evaluate whether it would have been more appropriate to exclude them from our survey. These "short ejecta" craters are distributed across the spectrum of planform types and are a modest fraction of the survey population, so their inclusion has a minor effect on our interpretations.

In summary, we consider the tabular results for the survey results for craters below 50°N to be representative of the production population for craters over 5 km in diameter. Table 2 summarizes these results and compares the transition angles inferred from Equation 1 with the transition angles for comparable forms in the experimental work of Gault and Wedekind (1978) and the lunar survey of Herrick and Forsberg (2003). Although emplaced as ramparts, the planforms of Martian ejecta blankets more closely resemble those for craters formed in a dry vacuum than they do Venusian craters, and the angular occurrence of impact forms is consistent with the analogous forms on the Moon and in the laboratory.

The similarity of Martian planforms to dry-vacuum craters includes some important details with respect to the uprange and downrange forbidden zones. The curving nature of the uprange forbidden zone and the sharp, straight-edged wedge of the downrange forbidden zone are a close match to the planform of the ballistically emplaced experimental highly oblique impacts in a vacuum (in particular, compare Fig. 1g to the 5° impact in Fig. 11a of Gault and Wedekind 1978). This similarity is particularly unusual when one considers that the ramparts, which are thought to represent the terminus of a surface flow, extend in a nearly perpendicular direction from the rim of the crater in Fig. 1g. Anecdotal

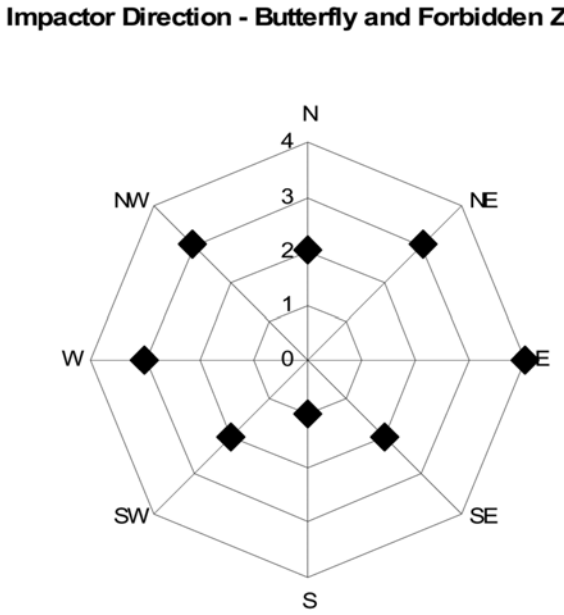

Fig. 6. The number of craters versus inferred impact direction for craters with butterfly and forbidden zone ejecta pattern.

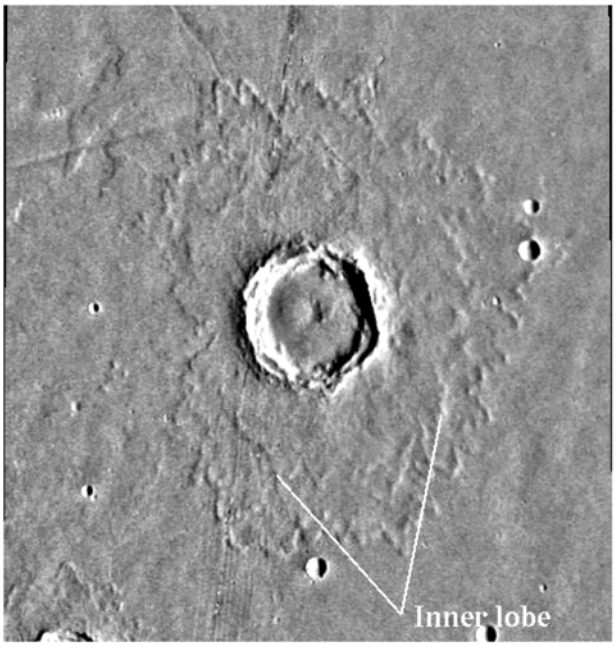

Fig. 7. An impact crater with an uprange forbidden zone (18.0°N, 142.5°E, D = 25 km, A = 81°). If erosion resulted in preservation of only the inner lobe of ejecta, then we would probably have classified this crater as type "offset."

observations of smaller Martian craters (Fig. 9) indicate that the nature of the uprange forbidden zone does not appear to change as crater diameter decreases below that for which ramparts form. At larger sizes, however, there is some indication that surface flow distorts the typical forbidden-zone planform (e.g., Fig. 1e).

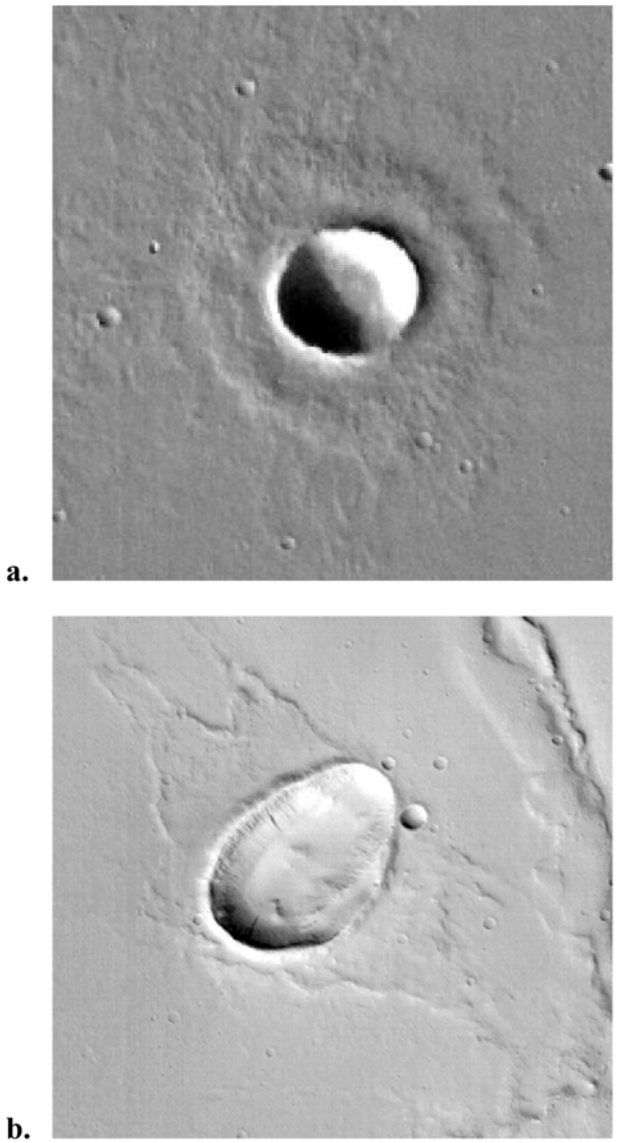

Fig. 8. Two craters with ejecta blankets of unusually short extent. a) A crater at 23.2°N, 281.6°E, D = 7 km, classified as "offset" in THEMIS imagery. b) The crater in Fig. 1h as imaged by the Mars High Resolution Stereo Camera (HRSC) at a resolution of ~20 m. Although (a) may be the erosional remnant of a larger ejecta blanket, the freshness of the crater in (b) suggests that the short blanket represents the full extent of the emplaced ejecta.

There are a couple of differences between Martian craters and dry-vacuum craters besides rampart formation. A detailed analysis of the topography of the Martian oblique impact forms is underway and not within the scope of this paper, but one significant difference from dry-vacuum craters is obvious even in the Viking imagery. Martian craters maintain an elevated uprange rim at all impact angles, while dry-vacuum impacts produce no uprange rim at low angles. Also, no Martian butterfly craters were observed that preserve a downrange ray, perhaps because this feature is easily eroded on Mars.

Table 2. Classification of Martian impact craters with $D > 5$ km for craters below 50°N latitude and compared to transition angles for craters from the laboratory experiments of Gault and Wedekind (1978) and the lunar craters surveyed with Clementine data in Herrick and Forsberg-Taylor (2003). Calculations as in Table 1.

Description	Number of craters	Cumulative fraction	90% CI	Transition angle	Lab impacts	Lunar
Butterfly	9	0.042	0.023	8–15°	5°	3–15°
Forbidden zone	10	0.090	0.033	14–21°	20°	23–33°
Offset and cross-range	8	0.128	0.038	17–24°	30°	n/a
Offset	51	0.370	0.055	34–41°	45°	38–48°
Symmetric	133	1.000				
Total	211					

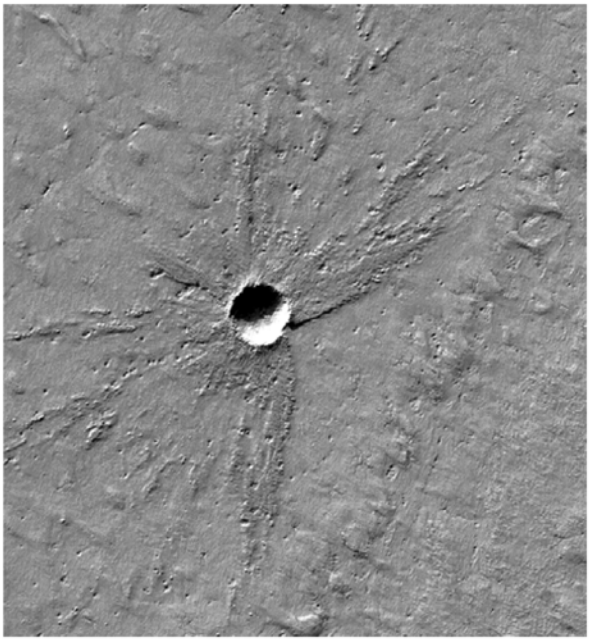

Fig. 9. A crater 280 m in diameter located at 86.3°S, 247.0°E as imaged by the Mars Orbiter Camera. Although this crater is much too small to have ramparts in the ejecta, the uprange forbidden zone is very similar in morphology to that observed in Fig. 1g.

CONCLUSIONS

Martian craters have similar ejecta planform that occur at similar impact angles to those observed in dry-vacuum settings. Although flow of the ejecta has occurred, the Martian craters otherwise show little similarity to oblique impact forms on Venus. It is difficult to reconcile the similarities with ballistically emplaced ejecta blankets with a mechanism for rampart formation that involves having the majority of ejecta flow outward from near the rim. The similarity with dry-vacuum craters suggests that Martian crater ejecta are predominantly ballistically emplaced. Ramparts then form as a result of modest, post-emplacement flows that preserve the basic ejecta planform.

Acknowledgments–This work was partially funded by NASA grant NAG5-12216 from the Mars Data Analysis Program. This paper was enhanced by reviews from Peter Mouginis-Mark, Nadine Barlow, and an anonymous reviewer. The full database of craters used in this study is available by request from R. Herrick.

Editorial Handling—Dr. Nadine Barlow

REFERENCES

Barlow N. G. 2000. Updates to the *Catalog of Large Martian Impact Craters* (abstract #1475). 31st Lunar and Planetary Science Conference. CD-ROM.

Barlow N. G. 2005. Martian impact craters as revealed by MGS and Odyssey (abstract #1415). 36th Lunar and Planetary Science Conference. CD-ROM.

Barlow N. G. and Bradley T. L. 1990. Martian impact craters: Correlations of ejecta and interior morphologies with diameter, latitude, and terrain. *Icarus* 87:156–179.

Barlow N. G., Boyce J. M., Costard F. M., Craddock R. A., Garvin J. B., Sakimoto S. E. H., Kuzmin R. O., Roddy D. J., and Soderblom L. A. 2000. Standardizing the nomenclature of Martian impact crater ejecta morphologies. *Journal of Geophysical Research* 105:26,733–26,738.

Barnouin-Jha O. S. and Schultz P. H. 1996. Ejecta entrainment by impact-generated ring vortices: Theory and experiments. *Journal of Geophysical Research* 101:21,099–21,115.

Barnouin-Jha O. S. and Schultz P. H. 1998. Lobateness of impact ejecta deposits from atmospheric interactions. *Journal of Geophysical Research* 103:25,739–25,756.

Barnouin-Jha O. S., Baloga S., and Glaze L. 2005. Comparing landslides to fluidized crater ejecta on Mars. *Journal of Geophysical Research*, doi:10.1029/2003JE002214.

Bottke W. F., Love S. G., Tytell D., and Glotch T. 2000. Interpreting the elliptical crater populations on Mars, Venus, and the Moon. *Icarus* 145:108–121.

Carr M. H., Crumpler L. S., Cutts J. A., Greeley R., Guest J. E., and Masursky H. 1977. Martian impact craters and emplacement of ejecta by surface flow. *Journal of Geophysical Research* 82: 4055–4065.

Gault D. E. and Wedekind J. A. 1978. Experimental studies of oblique impact. Proceedings, 9th Lunar and Planetary Science Conference. pp. 3843–3875.

Herrick R. R. and Forsberg-Taylor N. K. 2003. The shape and appearance of craters formed by oblique impact on the Moon and Venus. *Meteoritics & Planetary Science* 38:1551–1578.

Herrick R. R. and Phillips R. J. 1994. Effects of the Venusian atmosphere on incoming meteoroids and the impact crater population. *Icarus* 112:253–281.

Johnson R. R. 1973. *Elementary statistics.* North Scituate, Massachusetts: Duxbury Press. 480 p.

Passey Q. R. and Melosh H. J. 1980. Effects of atmospheric breakup on crater field formation. *Icarus* 42:211–233.

Pierazzo E. and Melosh H. J. 2000. Understanding oblique impacts from experiments, observations, and modeling. *Annual Review of Earth and Planetary Sciences* 28:141–167.

Schultz P. H. 1992a. Atmospheric effects on ejecta emplacement. *Journal of Geophysical Research* 97:11,623–11,662.

Schultz P. H. 1992b. Atmospheric effects on ejecta emplacement and crater formation on Venus from Magellan. *Journal of Geophysical Research* 97:16,183–16,248.

Schultz P. H. and Gault D. E. 1979. Atmospheric effects on Martian ejecta emplacement. *Journal of Geophysical Research* 84:7669–7687.

Schultz P. H. and Gault D. E. 1985. Clustered impacts: Experiments and implications. *Journal of Geophysical Research* 90:3701–3732.

Schultz P. H. and Lutz-Garihan A. B. 1982. Grazing impacts on Mars: A record of lost satellites. *Journal of Geophysical Research* 87: A84–A96.

Shoemaker E. M. 1962. Interpretation of lunar craters. In *Physics and astronomy of the Moon*, edited by Kopal A. New York: Academic Press. pp. 283–351.

Tanaka K. L., Skinner J. A., Jr., Hare T. M., Joyal T., and Wenker A. 2003. Resurfacing history of the northern plains of Mars based on geologic mapping of Mars Global Surveyor data. *Journal of Geophysical Research*, doi:10.1029/2002JE001908.